Astron. Astrophys. 329, 895–905 (1998)

ASTRONOMY
AND
ASTROPHYSICS

The evolution of dynamo maintained magnetic fields in a barred spiral galaxy

D. Moss[1], **M. Korpi**[2], **P. Rautiainen**[2], **and H. Salo**[2]

[1] Mathematics Department, University of Manchester, Manchester M13 9PL, UK
[2] Department of Geosciences and Astronomy, P.L. 333, University of Oulu, FIN-90571 Oulu, Finland

Received 25 April 1997 / Accepted 20 August 1997

Abstract. We model the evolution of dynamo maintained magnetic fields in a barred spiral galaxy. The velocity fields are taken from N-body dynamical simulations. The important feature is the presence of strong, unsteady non-circular gas motions, driven by the central bar, The nonlinear dynamo calculations are carried out with both two dimensional (thin disc approximation) and three dimensional codes. The resulting magnetic field shows repeated episodes with approximately ring-like structure, and structure with short spiral arms. These morphological features appear robust, in that velocity data from distinct dynamical simulations gives rise to similar structures.

Key words: MHD – galaxies: kinematics and dynamics – galaxies: magnetic fields – galaxies: spiral

1. Introduction

Spiral galaxies appear usually to host magnetic fields on both global and smaller scales, see e.g. the review by Beck et al. (1996). The determination of the detailed morphology of the large-scale fields is difficult (Beck et al. 1996), but it does appear that many possess approximately an axisymmetric structure, perhaps modified by features with azimuthal wave number $m = 2$ (i.e. an axisymmetric structure has $m = 0$). Others have significant $m = 1$ structure (bisymmetric spiral: BSS), and sometimes the picture may be more complicated. Note that current observational techniques are only adequate to determine the most prominent components of the field structure, and that it is plausible that higher order azimuthal components are quite generally present.

Basic dynamo theory (e.g Ruzmaikin, Sokoloff, Shukurov 1988, Eltsner et al. 1992, Moss & Brandenburg 1992) predicts that $m = 0$ fields are the most readily excited, and they appear also to be stable in the nonlinear regime (see, e.g., Moss et al. 1993a,b). A possible complication is that transients, reflecting the unknown initial conditions, may persist for several Gigayears, before the eventual stable configuration is achieved (Moss & Tuominen 1989, Brandenburg et al. 1992, Moss et al. 1993a, Poezd et al. 1993).

Thus finding an explanation for the maintenance of nonaxisymmetric magnetic features until the present epoch presents an interesting challenge for dynamo theory. The problem of explaining BSS has attracted considerable attention during the last few years. Apart from the possibility that it is a long-lived transient (Moss et al. 1993a), mechanisms investigated rely on nonaxisymmetries in the galactic disc. This can appear directly in the alpha-effect (Moss & Brandenburg 1992), perhaps involving parametric resonance or a related mechanism, or might arise from large-scale streaming velocities driven by the density wave associated with 'grand design' spiral arms (Chiba 1991, Mestel & Subramanian 1991, Subramanian & Mestel 1993, Schmidt & Rüdiger 1992, Moss 1995, Moss 1996a,b, Moss 1997, Bikov et al. 1997, and others), or from essentially impulsive galaxy-galaxy encounters (Moss et al. 1993a,b, Moss 1996b, 1997).

Barred spiral galaxies offer another example of a situation where large-scale nonaxisymmetric streaming velocities occur. Any dynamo generated field would be expected to be modified significantly by such motions, and hence to possess substantial nonaxisymmetric components. Chiba & Lesch (1994) presented a study of the effects of non-circular gas motions, of a type that might be associated with barred galaxies, on magnetic field generation and evolution. They used a quasi-local form of the induction equation, and made some quite drastic assumptions about the form of the non-circular velocities. Their very simplified model, together with the absence of any visualization of the resulting global field, make it difficult to assess readily their results, and to compare them with ours. In particular, it is unclear whether their field structures can be maintained against global decay in the absence of an α-effect.

Subsequently, Otmianowska-Mazur & Chiba (1995) also studied the inductive effects of steady large-scale gas streaming on galactic magnetic fields. Their velocities were generated by a SPH simulation of the motion of gas under prescribed nonaxisymmetric disturbances to a given potential. They also did not include any α-effect, and their calculations were strictly linear.

Send offprint requests to: D. Moss

The boundary conditions are unclear, but this presumably implies that their magnetic fields eventually decay. In most of the models presented, the disc plane value of the magnetic diffusion is very large (5×10^{27} cm^2 s^{-1}). In these, and other, ways their calculations differ from ours.

In this paper we study the behaviour of magnetic fields in the presence of velocity fields derived from numerical simulations of barred galaxies. We use the N-body code developed by Salo (1991; see also Salo and Laurikainen 1993, which describes the 3D version of the code), which follows the evolution of a self-gravitating galactic disc embedded in an analytically modelled spherical halo. The simultaneous evolution of both 'gas' and 'stars' is included, the former being represented by dissipatively colliding particles. Under suitable conditions a central bar can form, with associated large-scale gas streaming. We have taken the gas velocity fields from two such simulations in which the velocities are restricted to be two dimensional, and included them in both a 2D and a 3D galactic dynamo model, for times of up to nearly 10 Gyr. Most of the calculations presented are with the 2D version of the dynamo code, as shorter trial runs suggest that the global magnetic field morphology calculated with the 3D code is quite similar. The latter simulations are, of course, much more time consuming. However, for inclusion of velocity data from a 3D dynamical simulation, the 3D dynamo code will be essential.

Of course, a dynamical simulation from different initial conditions, and/or with other parameters changed would produce different velocities. We do not claim to give a unique description of magnetic field evolution during the formation and evolution of a galactic bar, nor even to model processes occurring in any particular galaxies. We do think that we can display some of the morphological features of the magnetic fields that arise.

2. The dynamo model

We take a standard mean field dynamo equation

$$\frac{\partial \mathbf{B}}{\partial t} = \nabla \times (\mathbf{u} \times \mathbf{B} + \mathbf{u}_{\rm dia} \times \mathbf{B} + \alpha \mathbf{B} - \eta \nabla \times \mathbf{B}) \,. \qquad (1)$$

As usual, η is the turbulent magnetic diffusivity and α represents a conventional alpha-effect. $\mathbf{u}$ comprises the large-scale velocities (circular and non-circular), $\mathbf{u}_{\rm dia} = -\frac{1}{2}\nabla\eta$, and represents the turbulent diamagnetism (Vainshtein & Zeldovich 1972, Roberts & Soward 1975). In general we allow $\alpha = \alpha(\mathbf{r})$, $\eta = \eta(\mathbf{r})$. We solve eqn (1) as either a 2D or a 3D initial value problem. Initial conditions were usually that the seed field be axisymmetric and of low energy compared to the saturation value. For the 3D calculations, it is also localized near the disc plane. However the initial configurations are rapidly forgotten as the simulations proceed. The 3D version of the code allows $\mathbf{u}$, α and η to vary also with z, the coordinate perpendicular to the disc plane. Note that both the 2D code (implicitly) and 3D (explicitly) can only consider fields of even (quadrupolar) parity with respect to to disc plane $z = 0$. Given that the currently used velocity data is two dimensional, and that theory and observation predict that fields of quadrupolar parity are generally to be expected, we feel that this is not a fundamental restriction at this time. Nevertheless, we recognize the desirability of implementing a more general code, especially if we wish to use truly 3D velocity data. For computational convenience we put

$$\mathbf{u} = \Omega(r) r \hat{\phi} + \mathbf{v}, \qquad (2)$$

thus separating the circular and non-circular velocities. In general we write $\alpha = \alpha_0 \tilde{\alpha}(\mathbf{r})/(1 + \alpha_{\rm B}\mathbf{B}(\mathbf{r})^2/B_0^2)$, $\eta = \eta_0 \tilde{\eta}(\mathbf{r})$, $\mathbf{v} = v_0 \tilde{\mathbf{v}}(\mathbf{r})$, with α_0, η_0 and v_0 being typical values of α, η and $|\mathbf{v}|$ respectively. Thus $\alpha_{\rm B} = 1$ gives a basic form of α-quenching with field strengths limited at approximately B_0. Plausibly B_0 would be the field strength in equipartition with a typical value of the kinetic energy of the turbulent velocities. Alternatively, $\alpha_{\rm B} = 0$ would yield a linear calculation. A more sophisticated model might have $B_0 = B_0(\mathbf{r})$, representing the change in the magnetic field-gas equilibrium condition as the gas density and turbulent velocity vary with position.

We make the conventional assumption that $\eta \approx \frac{1}{3} u_t l_t$, where u_t and l_t are typical values of the velocity and length scale of the turbulence. In the Milky Way, near the disc plane, $u_t \sim 10\,{\rm km\,s^{-1}}$, $l_t \sim 100\,{\rm pc}$, gives an estimate for η of about $10^{26}\,{\rm cm^2\,s^{-1}}$. However conditions in the sort of galaxies we are considering may be rather different, and the above expression for η is only an order of magnitude estimate, so the value of η is rather uncertain. η_0 is chosen to be equal to or slightly greater than the maximum value of η, so that $\tilde{\eta} \leq 1$. We can define the corresponding magnetic Reynolds numbers $R_\alpha = \frac{\alpha_0 L}{\eta_0}$, $R_{\rm m} = \frac{v_0 L}{\eta_0}$, where L is a convenient length scale, either h (a measure of the disc thickness) or R (the disc radius) – see below. We define $v_0 = 1\,{\rm km\,s^{-1}}$, and choose α_0 such that the maximum value of α is approximately 1-5 ${\rm km\,s^{-1}}$, and η_0 satisfies $10^{26} \lesssim \eta_0 \lesssim 6 \times 10^{26}\,{\rm cm^2\,s^{-1}}$. Note (Sect. 6) that the local value of η only approaches the largest of these values of η_0 in the 3D calculations high in the halo. In principle, $R_{\rm m}$ is fixed exactly by the dynamo model parameters, but in practice we explore the effects of modest changes in this parameter. We always use the nominal value of the circular velocity Ωr, and so the other conventional dynamo parameter, $R_\omega = \Omega_0 L^2/\eta$, is fixed by the dynamical model via eqn (2). Lengths are scaled with R, the disc radius, and units of time are $L^2/\eta_0 = T$, say.

2.1. The 2D model

The 2D 'no-z' approximation is based on the idea of replacing z-derivatives by terms $\sim O(h^{-1})$, where h is the disc thickness or scale height (e.g. Subramanian & Mestel 1993, Moss 1995), and the code is in the form implemented in Moss (1996), solving a modified version of Eq. (1) on $0 \leq r \leq R$, $0 \leq \phi \leq 2\pi$, with $NI \times NJ$ grid points and uniform meshing.

We assume that η is uniform, i.e. $\tilde{\eta} = 1$ and, for most of the computations, $\tilde{\alpha} = 1$ also. The length scale L is taken as h. Boundary conditions are that $B_r = B_\phi = 0$ at $r = R$. Results were little affected for other plausible choices of boundary condition, provided that R was large enough for the dynamo-active region to be included within the computational domain.

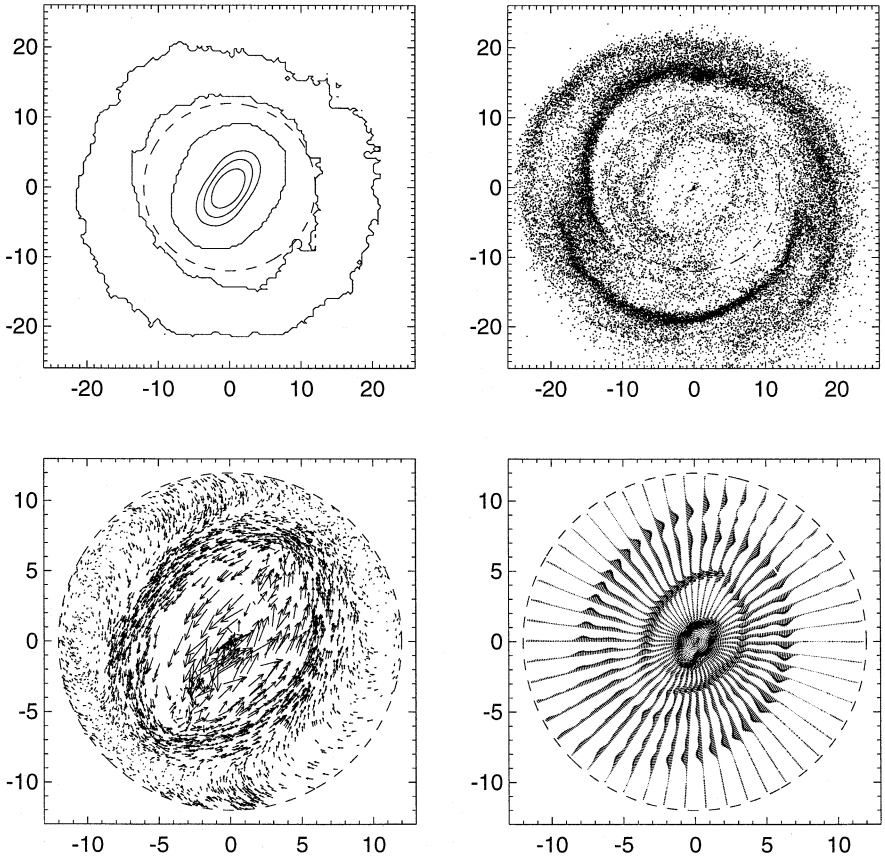

Fig. 1. Snapshots from the 2D model I calculation at time 2.2 Gyr. In the upper row, the left and right hand panels give the density contours of the stellar density distribution and the gas particle positions, respectively. The lower left panel shows the gas velocity vectors in a coordinate system that co-rotates with the bar, and on the right the corresponding magnetic field vectors are shown. The dashed outer circle in each frame is drawn at a radius of 12 kpc, the outer boundary of the MHD calculation.

2.2. The 3D model

The 3D code is described in Moss (1997), and comparisons are there made with the 2D code. Eq. (1) is solved on a grid of size $NI \times NJ \times NK$ covering $0 \leq r \leq R$, $0 \leq \phi \leq 2\pi$, $0 \leq z \leq z_{\max}$. The spacing is uniform in each of the coordinate directions. We found that taking $z_{\max} = (0.4 - 0.5)R$ produced fields at this boundary that were small compared to their maximum values, and that results were insensitive to increasing $z_{\max}$ further. Mostly we considered $\tilde{\alpha}$ and $\tilde{\eta}$ only to vary with z, and we took, slightly arbitrarily,

$$\begin{aligned} \tilde{\alpha} &= z(z_\alpha^2 - z^2), & z \leq z_\alpha, \\ \tilde{\alpha} &= 0, & z > z_\alpha, \\ \tilde{\eta} &= \eta_1 = \text{constant}, & z < z_\eta, \\ \tilde{\eta} &= 1, & z > 2z_\eta, \end{aligned} \tag{3}$$

with $\tilde{\eta}$ varying smoothly between $z = z_\eta$ and $2z_\eta$. It is the z-dependence of these quantities that effectively defines the disc. Thus the disc plane value of η is $\eta_1\eta_0$. It is plausible that the diffusivity is larger in the halo than in the disc (eg Sokoloff & Shukurov 1990), and we thus take $\eta_1 < 1$. We set $L = R$ for the scalings. We arbitrarily prescribed a decrease in the size of the non-circular gas velocities as z approached $z_{\max}$.

Our boundary conditions are that on $z = z_{\max}$ B_r and B_ϕ should be decreasing in magnitude at least as fast as for a general dipolar field. Similar 'open' conditions are applied on $r = R$, and the condition on the third field component is found by satisfying $\nabla \cdot \mathbf{B} = 0$. As for the 2D calculations, we verified that plausible variations in these boundary conditions, such as setting some field components to zero at the boundary, did not alter significantly our results.

The restriction to uniform mesh size in the z-direction does mean that it is not possible to investigate discs of aspect ratio as small as those of real spiral galaxies, with the computing resources available. Practically, we are limited to $\lambda \gtrsim 0.1$. With the 2D velocity data this is probably not a real limitation when investigating the generation of nonaxisymmetric structure. However, we will obviously represent less well the z-structure of the fields.

3. Summary of the dynamical calculations

The velocity fields for the dynamo program are generated by the N-body simulation code described in Salo (1991) and Salo and Laurikainen (1993). In the current simulations the gravitational potential was determined on a 2-dimensional logarithmic polar grid, with 108 azimuthal and 144 radial cells. The stellar component consists of 200 000 self gravitating particles, initially distributed in an exponential disc. The gravitational softening parameter ϵ was $\frac{1}{8}$ of the scale length, taken to be 3 kpc, and the initial value for Toomre's Q_T -parameter was 1.0. The gas component is modelled by 40 000 inelastically colliding test particles: in each impact the normal component of the relative velocity of the colliding particles is reversed, and multiplied by the coefficient of restitution, taken to be 0.2. The initial random

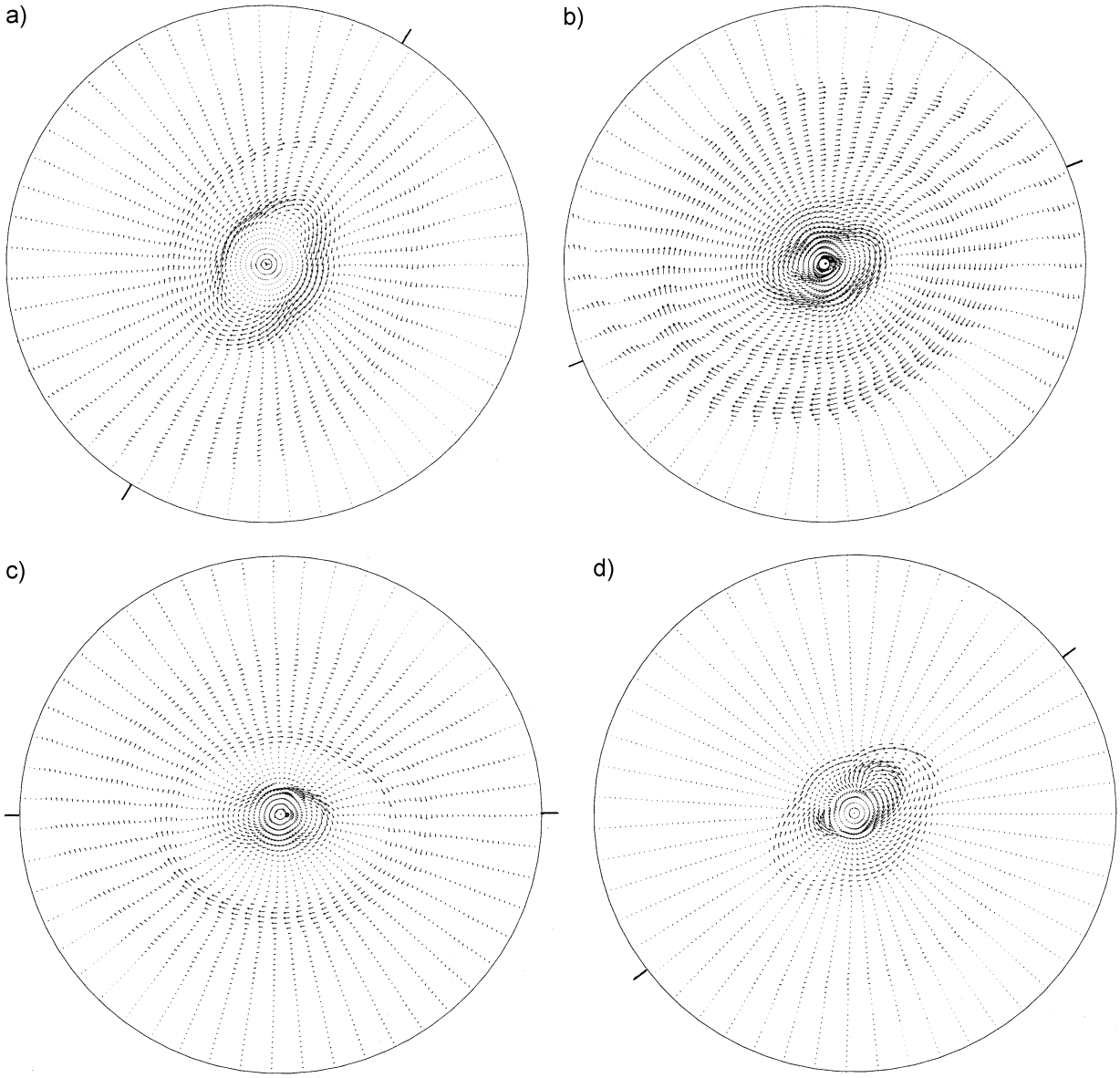

Fig. 2. Snapshots of magnetic field for the case with R = 12 kpc, $\eta_0 = 2 \times 10^{26}$ cm^2 s^{-1}, $R_{\rm m}$ = 0.25.at times 0.6, 1.2, 2.8, 4.0, 4.6, 6.0, 6.6, 8.4 Gyrs. The radii projecting beyond the circumscribing circle (the outer computational boundary at r = 12 kpc) indicate the current position of the bar axis.

velocities of the gas particles were 5% of the circular velocity. The analytical halo is represented by an isothermal sphere potential.

Two different models were used that differed only in their disc-halo mass relation. In the first (Model I) the disc mass fraction (measured within 4 exponential scale lengths = 12 kpc of the centre) was 68%. This means that the disc dominates the rotation curve and the initially axisymmetric simulation system develops a strong bar that gives rise to strongly noncircular velocities. This results in a high gas cloud collision frequency, which leads to inflow and eventually leaves 'holes' in the gas distribution. This is undesirable from the point of view of dynamo calculations (see Sect. 4) but perhaps corresponds to the situation in many barred galaxies: the bar area is often relatively deficient in neutral hydrogen – see, for example, NGC 1365 (Lindblad et al. 1996), NGC 1300 (Lindblad & Kristen 1996) and NGC 1433 (Ryder et al. 1996). In addition to this inflow, the gas component forms inner and outer rings which are related to resonances (Schwarz 1981, Byrd et al. 1994), and are often observed in barred galaxies (Buta 1995).

In the second model (Model II) the disc mass fraction was reduced to 41% (again measured within 12 kpc). The amplitude and the shape of the rotation curve are very similar to those of the first model, but now the halo dominates the initial rotation curve through most of the disc region except near the middle of the disc. The effect of the bar on the overall dynamics is much

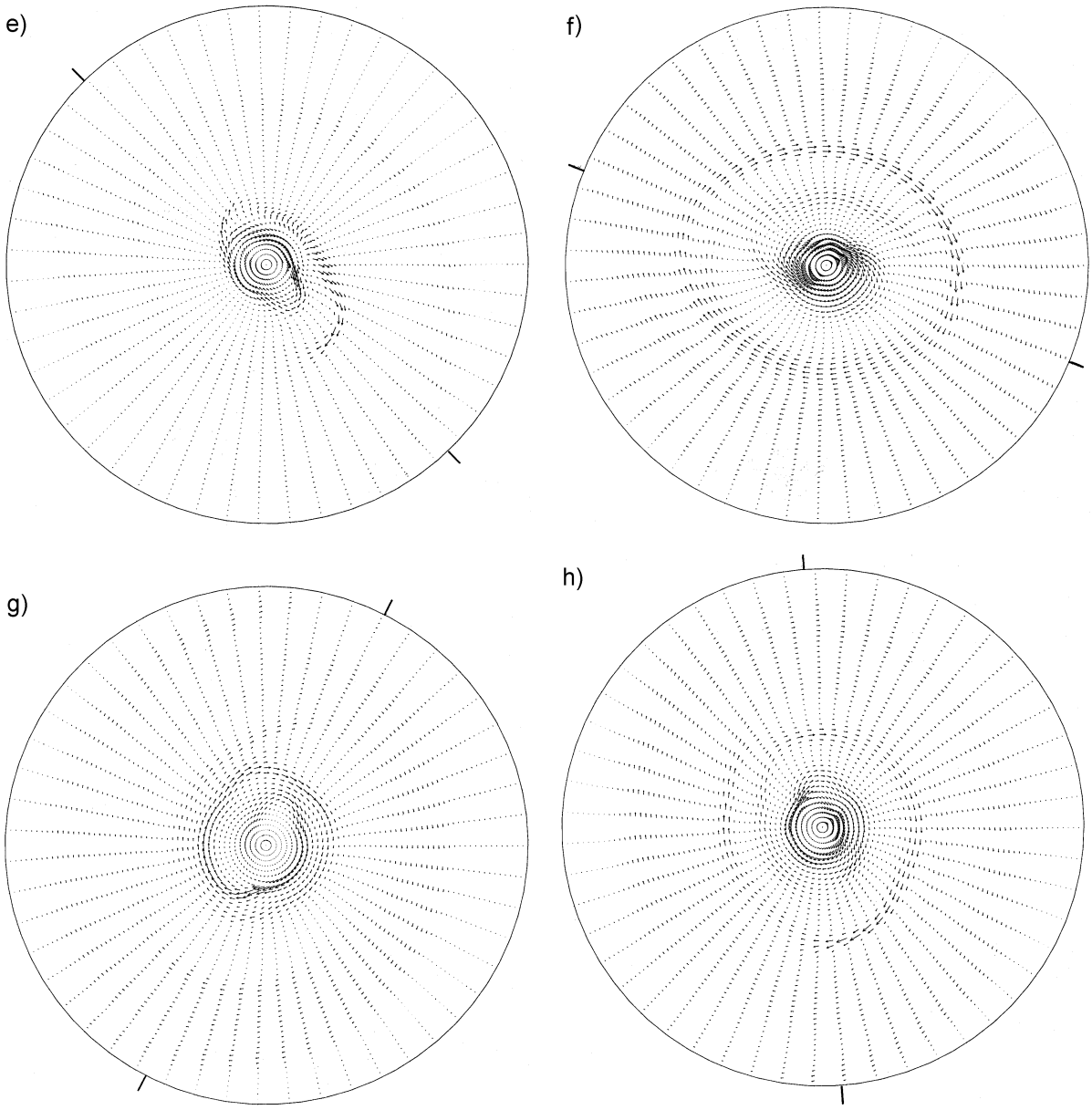

Fig. 2. (continued)

smaller, and so the inflow of gas is not as strong as in model I. There is an inner gas ring but globally the spiral structure resembles a multiarmed galaxy. No outer gas ring is formed.

It is important to note that the magnetic induction is not directly affected by variations of the simulated gas density, but depends only on the gas velocity field, the streaming motions being determined by the strength of the bar. In Model I the gas motions are essentially non-circular, while in Model II the deviations from the circular motion are of the order of 50%. The latter figure is consistent with observed non-circular motions, whereas the former model is perhaps only applicable to the most extreme cases. In what follows we mostly concentrate on model I: however, for reasons discussed below we have effectively reduced the values of the non-circular velocities used in our computations (see Sect. 5).

Numerical simulations indicate that the pattern speed of the bar decreases due to angular momentum exchange between the bar and the outer galaxy (this was already noticed by Sellwood 1981). In our present models this decrease is not high, only 17% during the whole evolution of model I (excluding the initial bar formation period). Similarly, the amplitude and shape of the bar show only little evolution. However, if our halo, as well as the disc, consisted of self gravitating particles, this would provide an additional interaction mechanism, and the slow-down of bar would probably then be faster (Little and Carlberg 1991). Including this effect would require a three-dimensional simulation, and could also show other evolutionary phenomena that are not seen in the present simulations.

An snapshot of the dynamical models is given in Fig. 1, where the stellar and gas distributions in Model I are shown

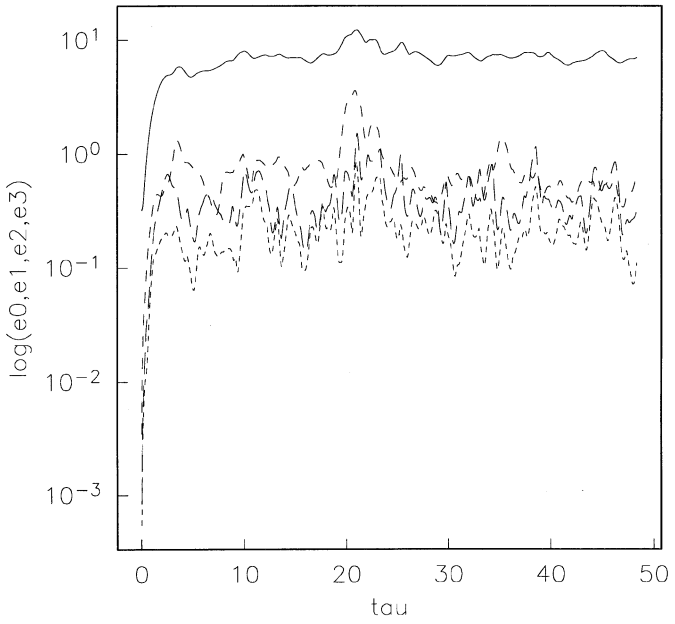

Fig. 3. Variation of energies in modes $m = 0, 1, 2, 3$ (respectively continuous, long-dashed, medium-dashed, short-dashed curves) with time for case in Fig. 2. The time unit is 0.21 Gyr.

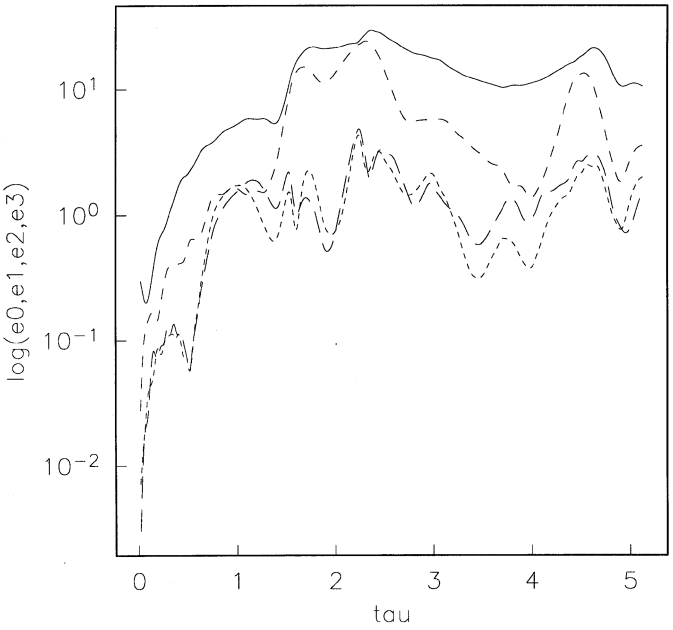

Fig. 4. As Fig. 3, but for a calculation with R = 7.5 kpc.

about 2 Gyr after the MHD simulation was started. The gas particle velocities are also shown (in a frame co-rotating with the bar), and the magnetic field vectors at the same time, from the simulation described in Sect. 5.1.

We have not tested how the details of the velocity field would change if different methods (Smoothed Particle Hydrodynamical or a fluid dynamical treatment) were used. However, as similar morphological features (resonance rings, shock regions) are typically obtained in simulations with various methods (compare for example Schwarz 1981, Friedli and Benz 1993, Lindblad et al. 1996), there is no reason to assume that the accompanying velocity fields would be drastically different. Also, taking into account our current poor knowledge of the behaviour of ISM, none of the three methods can be preferred over the other two (Sellwood and Wilkinson, 1993).

4. Reduction of velocity data

The raw velocity data from the dynamical model is Lagrangian, with pairs of (x, y) and (v_x, v_y) being associated at each time with each gas 'particle'. The dynamical simulation described in Sect. 3 results in strong streaming and thus localization of the gas, and there are regions, especially at small radii, where gas velocity data (v_x, v_y) are sparse or absent. Also there is a significant dispersion in these velocities (although less than for the 'star' particles). These facts mean that some care is needed to produce an accurate and well-behaved representation of the velocities for incorporation into the dynamo codes. We do not use velocity data from the initial transient period of the dynamical calculations, when the bar is forming.

We made considerable experimentation before choosing the procedure described immediately below as Method 1 for the main calculations described below. It certainly is not unique. However we feel that it is reasonably robust in that a rather different procedure, Method 2, gives a quite similar dataset. Also, the gross features of the derived velocity fields, such as mean rotation curves, seem to be satisfactorily reproduced.

The accuracy of our interpolation is improved by storing data values with respect to the current position of the bar, and using the position angle of the bar as an additional datum when reconstructing the velocity field in the inertial frame.

We also outline a rather less sophisticated treatment of the velocity data as Method 3, and discuss simulations using this algorithm briefly in Sect. 5.

All the processes described here involve substantial smoothing of the data. This is not only necessary to produce velocity fields that are sufficiently smooth for the dynamo codes to operate satisfactorily, but is also consistent with the principles of mean field theory.

4.1. Method 1

We choose the radius R within which we will make the dynamo calculation (typically 7.5 or 12 kpc, see Sect. 2), and ignore all data from outside this radius. We then choose a uniform radial and azimuthal meshing, of size $nr \times np$ say, and determine mean values, v_r, v_ϕ of the radial and azimuthal velocity components in each of the 'boxes' defined by this mesh.

Typically there are a number of 'holes', i.e. boxes with no data, mainly in the inner part of the disc. We minimize the problem, and also reduce the noise, by choosing relatively small values of nr and np; $nr = 21, np = 41$ were found to be reasonable values when R = 7.5 kpc, and $nr = 33$ was used when R = 12 kpc. We then 'patch' the holes by giving them velocity values that are naive averages of those of neighbouring boxes.

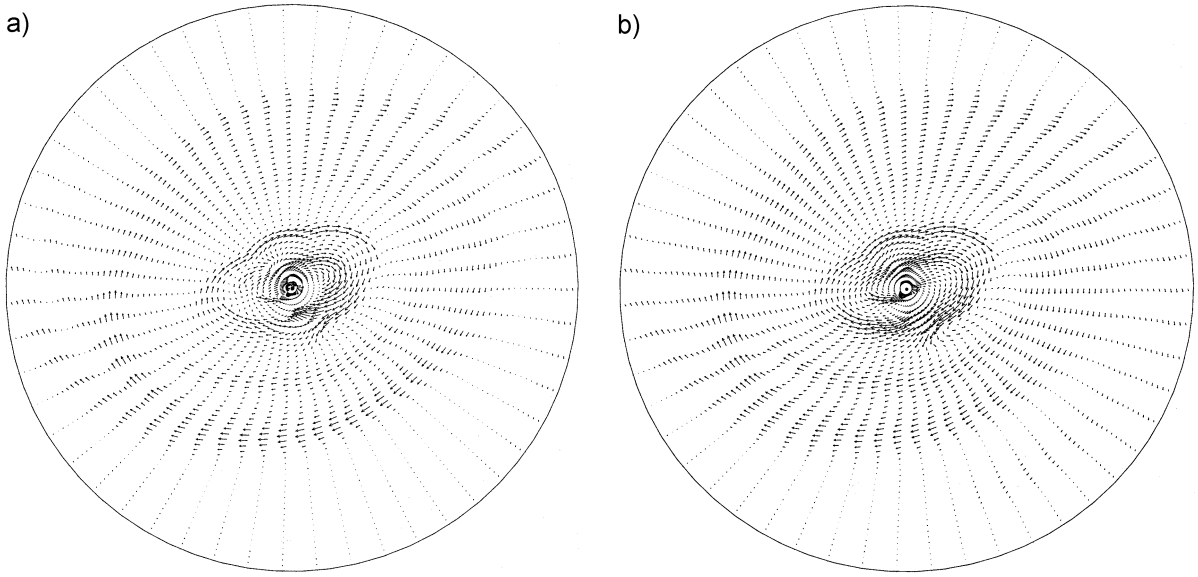

Fig. 5a and b. Snapshots of field structure at time 1.2 Gyr, $R_\alpha = 1$ for **a** $R_m = 0.4$, $\eta_0 = 2 \times 10^{26}$ cm^2 s^{-1};**b** $R_m = 0.2$, $\eta_0 = 4 \times 10^{26}$ cm^2 s^{-1};

The next step is to Fourier analyse these values of $v_{\rm r}$ and v_ϕ for each radial ring. This produces complex Fourier coefficients, $v_{\rm rm}$(r), $v_{\phi{\rm m}}$(r) for $0 \le r \le R$, $0 \le m \le M$. Finally we perform a three-point radial smoothing on all the $v_{\rm rm}$ and $v_{\phi{\rm m}}$. The Fourier analysis thus serves two purposes. It gives an effective azimuthal smoothing, and it reduces the quantity of data needed for input to the dynamo code to a manageable quantity.

The data is stored at each time point (45 points cover 10 Gyr), and the dynamo code interpolates on the Fourier components in space and time and then reconstructs the two dimensional velocity field.

4.2. Method 2

This used a relatively high spatial resolution ($nr = np = 80$), in contrast to that described above. The effect of the holes was reduced by employing a weighted mean filtering procedure, in the radial direction. The velocity components at the mesh point (i, j) were determined by the algorithm

$$< v_{i,j} >= w_{i,j} v_{i,j} + (1 - w_{i,j}) \frac{v_{i+a,j} + v_{i-a,j}}{2} \qquad (4)$$

The weights $w_{i,j} = n_{i,j}/N_{\rm max}$, where $n_{i,j}$ is the number of data points present in the box (i, j), $N_{\rm max}$ the maximum number of datapoints present in any box, $v_{i,j}$ is the raw mean velocity component at (i, j) and $v_{i+a,j}, v_{i-a,j}$ are the first non-zero values of the raw mean after/before (i, j). In addition to reducing the effect of the holes, this also gives an effective radial smoothing. A standard FFT algorithm was then applied azimuthally, and proved to be quite effective in smoothing the noise in the data

4.3. Method 3

Using $nr = 21, np = 41$ with $R = 7.5$ kpc, we calculated average values in the grid boxes, as for Method 1. The only further process was to apply the smoothing

$$< v_{i,j} >= \left(v_{i-1,j} + v_{i+1,j} + v_{i,j-1} + v_{i,j+1} + 4v_{i,j}\right)/8 \qquad (5)$$

twice in succesion. There was thus no Fourier analysis, and the dynamo code performed spatial interpolation in two dimensions on the stored values. Our motivation for this procedure was to preserve more accurately the marked streaming evident in the dynamical calculations, especially by making the azimuthal smoothing rather more local.

5. Two dimensional calculations

Most of these simulations were performed with a grid defined by $NI = NJ = 101$, but some were repeated at higher resolution to verify that these values were large enough. We adopted standard galactic parameters of $R = 12$ kpc (4 exponential scale lengths), $h = 375$ pc (equal to the gravity softening parameter in the dynamical calculations), so the disc aspect ratio is $\lambda = h/R = 0.03125$. Thus with canonical values of $\eta = \eta_0 = 10^{26}$ cm^2 s^{-1}, $\alpha_0 = v_0 = 10^5$ cm s^{-1}, we obtain $R_{\rm m} = R_\alpha = 1.1$.

5.1. The main calculations

We used as standard velocity data that from the first calculation described in Sect. 3 (Model I), reduced by Method 1, including azimuthal Fourier components $m = 0 - 5$. We did verify that the results were not radically changed by taking M (Sect. 4) to be 3.

We attempted firstly to complete a simulation over 10 Gyrs with $\eta = 10^{26}$ cm^2 s^{-1}, $R_{\rm m} = R_\alpha = 1$, i.e. approximately the values quoted above. We encountered several situations, at intervals of 1-2 Gyr, when the interpolated non-circular velocities, in particular the radial component, became especially large at smaller radii. This resulted in the magnetic field being swept rapidly to the centre of the disc, and the numerical scheme eventually became unstable. (The problem can be somewhat alleviated by using a finer spatial mesh, but it appears that higher than practical spatial and temporal resolution would be needed

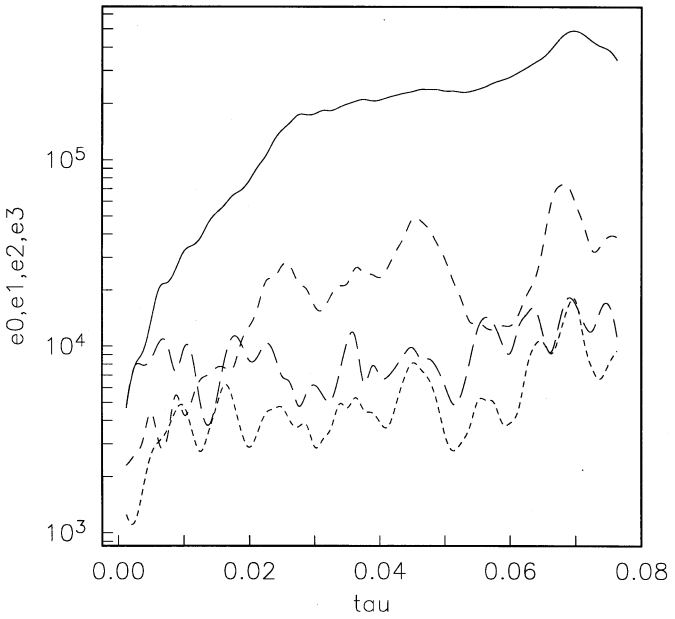

Fig. 6. Variation of energies in modes $m = 0, 1, 2, 3$ for 3D calculation described in Sect. 6. The unit of time is 28 Gyr.

to remove it altogether.) We thus adopted two methods to circumvent this problem, which probably is connected with the spatial sparsity of the raw velocity data (see Sect. 4. Either we arbitrarily reduced the magnitude of the non-circular velocities slightly, by reducing $R_{\rm m}$ to 50 or 80% of its nominal value, or we increased the diffusion coefficient, to $\eta_0 = 2 \times 10^{26}$, and, for comparison, also to 4×10^{26} cm s^{-1}. Of course, we can also use a combination of these two changes. When we increase η_0, we keep $R_\alpha = 1$, ie we increase the value of α_0, in order to ensure that a dynamo is still excited. We found that the gross features of the field evolution were very similar in all cases. Increasing the diffusion means (unsurprisingly) that the field features are somewhat broader. Both of these changes mean that the field concentration to the centre is reduced during episodes of strong radial velocities. Also, we note that, during intervals when the code does run satisfactorily with the canonical parameter values, then the results are again quite similar to those obtained with these modified values. As it may be that the local sparsity of the raw velocity data causes the interpolation process somewhat to exaggerate the radial velocities (Sect. 4), we consider either of these proceedures to be reasonable. We also verified that, when R_α was set to zero, the magnetic fields did decay; that is there is no 'false' dynamo effect arising from our representation of the imposed nonaxisymmetric velocities or boundary conditions.

We now discuss in more detail a simulation with $\eta_0 = 2 \times 10^{26}$ cm^2 s^{-1}, $R_{\rm m} = 0.25$, $R_\alpha = 1.0$ (i.e. a reduction of $R_{\rm m}$ to 50% of its nominal value). Projections of the magnetic field vectors on to the disc plane at successive times are shown in Fig. 2. The position of the axis of the bar is shown by the radii projecting beyond the circle representing the computational boundary. Ring and spiral-like structures appear and disappear, and at certain epochs (e.g. near time 4.6 Gyr), the field is concentrated near the centre of the disc. Fig. 1 shows the relation of the streaming velocities to the bar at a typical instant, and also shows the relation between the vectors of the magnetic field and streaming velocities. This is typical of our solutions.

Fig. 3 shows plots of the energies in azimuthal modes $m = 0, 1, 2, 3$ against time. In these plots, the $m = 0$ mode is clearly dominant. This might appear a little surprising given the nature of the field plots in Fig. 2. However, there are large parts of the disc where the field is predominantly axisymmetric, and the rather more striking nonaxisymmetric features are quite localized. This is more clearly seen in a short trial run with $R = 7.5$ kpc, with a slightly different velocity field to that used for the calculations described above. This excludes much of the region where the field is approximately axisymmetric, and accordingly gives larger relative energies in modes $m > 0$ – see Fig. 4. (Note that here the scale for the energies differs from that of Fig. 2.) In general, the global magnetic energy in the mode $m = 1$ is rather less than in $m = 2$, and that these contributions fluctuate quite strongly, see Fig. 3.

For comparison, in Fig. 5 we show field configurations at time 1.2 Gyr for simulations with parameters $R_m = 0.4$, $\eta_0 = 2 \times 10^{26}$ cm^2 s^{-1} (Fig. 5a), and $R_m = 0.20$, $\eta_0 = 4 \times 10^{26}$ cm^2 s^{-1} (Fig. 5b), both with $R_\alpha = 1$. Thus in Fig. 5a, the value of the noncircular velocities is closer to the 'raw' value, to be compared with the smaller values of the standard case (Fig. 2). In Fig. 5b the velocities again are nearer to their raw values, but η_0 is increased (remember that $R_m \propto \eta_0^{-1}$).

It is clear that the larger value of η_0 adopted for Fig. 5b tends to give rather broader magnetic features and increasing the value of R_m for fixed η_0 has the opposite effect. Note that, although in the case illustrated in Fig. 5b we have increased α_0 in keeping $R_\alpha = 1$, this has little effect on the field geometry.

5.2. Test with Method 3 velocities

We performed a limited comparison between results obtained using velocity data obtained by use of procedures 1 and 3. For this we took a time independent velocity field, corresponding to an early epoch of the simulation, and followed the evolution of the magnetic field for about 2 Gyr. The magnetic structures obtained showed strong similarities, but for the same parameter values those obtained with the Method 3 velocities were spatially narrower and generally (and not unexpectedly) exhibited rather more shearing.

5.3. Results using data from the Model II dynamical simulation

We also investigated magnetic field evolution, using data from the second simulation described in Sect. 3. We used the same procedure as for the two dimensional calculation described in Sect. 5.1. Clearly, the detailed results were different. However we found that the same general features of magnetic field morphology appeared, namely ring-like and short armed structures, with vectors of magnetic field and non-circular velocities well aligned.

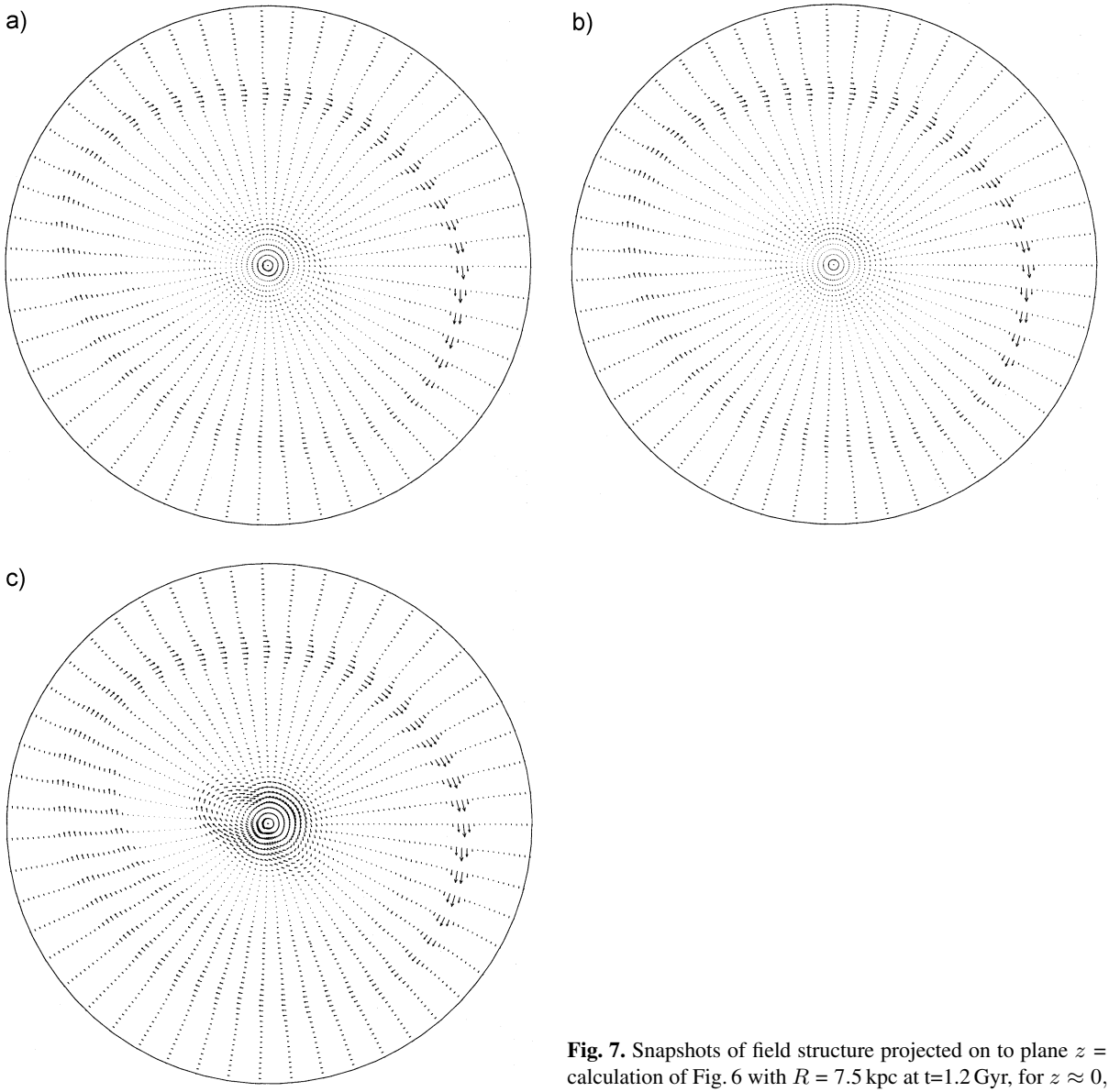

Fig. 7. Snapshots of field structure projected on to plane z = constant for 3D calculation of Fig. 6 with R = 7.5 kpc at t=1.2 Gyr, for $z \approx 0, 100, 200$ pc.

6. Three dimensional calculations

In this section we discuss only results obtained using the Model I velocities. We attempted to compare the results described in Sect. 5.1, obtained by using the 2D code, with those from a comparable calculation, for the same velocity data, using the 3D code. After some experimentation we adopted parameter values $z_\eta = 0.15R$, $z_\mathrm{m} = 0.4R$, $z_\alpha = 0.2R$, $\eta_\mathrm{l} = 0.333$, $\eta_0 = 6 \times 10^{26}\,\mathrm{cm^2\,s^{-1}}$, $R = 7.5\,\mathrm{kpc}$ for the simulations described below. Thus the value of η in $z \le z_\eta$ is $2 \times 10^{26}\,\mathrm{cm^2\,s^{-1}}$. It is plausible that the halo values of η may be rather larger than $6 \times 10^{26}\,\mathrm{cm^2\,s^{-1}}$, but we chose the above value for computational convenience (smaller values of η_l require a finer z-mesh). However our results are not very sensitive to the precise values of these parameters. We set $R_\mathrm{m} = 2.75$, close to, but a little reduced from, the nominal value, of 3.75 and $R_\alpha = 500$ corresponds to a maximum value of α of $1.5\,\mathrm{km\,s^{-1}}$ at $z \approx 0.12R$. The integration grid had $NI = NJ = 101$, $NK = 41$.

The code was run for approximately 2 Gyr using the Method 1 reduction of the raw velocity data. For these calculations we used the velocity field mentioned in Sect. 5.1 in connection with Fig. 3, that is a slightly modified form of that used for the majority of the calculations using the 2D dynamo code. The evolution of the global energies in the azimuthal modes is shown in Fig. 6, (the normalization cannot be directly compared with that of the two dimensional calculations), and Fig. 7 gives projections of the magnetic field vectors onto planes z = constant for several heights above the disc plane at time 1.2 Gyr. (Note that the length of the arrows representing the magnetic field vectors have been normalized to the maximum field strength present in each plot, and so the figures cannot be used directly to compare field strengths at different values of z.) A 2D calcula-

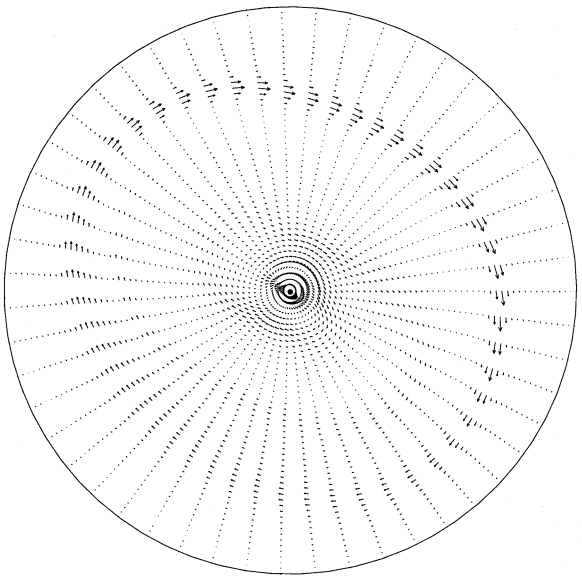

Fig. 8. Snapshot of field structure for 2D run with parameters approximating those of Fig. 7, at t=1.2 Gyr.

tion with broadly similar parameters (R = 7.5 kpc), except that $\eta_0 = 10^{26}\,\mathrm{cm^2\,s^{-1}}$, can be used for comparison. The evolution of the modal energies is shown in Fig. 4, and can be compared with those shown in Fig. 6, and the field structure for this run at 1.2 Gyr, given in Fig. 8, can be compared with the various panels of Fig. 7. Although clearly the field structure in the 3D case does depend on z, and the diffusion is larger in that case, the plots in Figs. 4 and 6, and those in Figs. 7 and 8 possess sufficient similarities to suggest that little additional information on the r, ϕ structure of the fields is being revealed by the 3D simulation. Thus we did not pursue these 3D calculations further.

7. Discussion and conclusions

An inherent problem with 2D dynamical simulations of the type described in Sect. 3 is that the dissipation is rather too large, and this may result in overestimation of the radial velocities. This appears to be one, at least, of the reasons why we found it necessary to reduce the value of R_m from its canonical value. Nevertheless, we are encouraged by the general robustness of our results. The main features of the magnetic field structure displayed in Fig. 2 persist when both the dynamo parameters and the velocity data reduction method are altered. Moreover, the same *general* (but not particular) features appear in the magnetic field structure when we use velocities from a dynamically distinct simulation (Sect. 5.3). Moreover our 2D dynamo model appears to capture the essential features of a more general, 3D, calculation, at least with the 2D velocity data. This has enabled an exploration of parameter space at reasonable computational cost. Nevertheless, the 3D code will certainly be needed when we use data from a 3D dynamical simulation.

We have chosen the simplest possible representation of the α-effect – that α is a scalar that does not vary with r and ϕ. More plausibly, $\alpha \propto \Omega(r)$, or even is proportional to the local vorticity (e.g. Brandenburg and Donner 1997). Test calculations with α proportional to the vorticity show that the overall changes introduced in the field structure are small. These and other experiments support the idea that in our simulations the magnetic field structure is almost completely determined by the recent history of the gas velocity field – see Fig. 1. Field lines closely follow streamlines. In this, our results are consistent with those of Otmianowska-Mazur & Chiba (1995). An α-effect is essential to prevent overall field decay, but relatively small field variations caused by changes in the form of α are masked by advection by the strong noncircular velocities.

Whilst our model does not purport to represent any 'real' spiral galaxy, we believe that it possesses some generic features, and that the general features of the magnetic field structure – appearance and disappearance of rings and short arms, a mixture of m = 1 and m = 2 nonaxisymmetric structure, etc – may be widely valid. This view is supported by the overall similarity between the dynamo calculations described in Sects. 5.1 and 5.3. An interesting and important step would be to model a barred galaxy for which both good quality velocity and magnetic data are available.

Acknowledgements. DM thanks the Dept of Geosciences and Astronomy, University of Oulu, for its hospitality. The work was partially supported by SERC/PPARC Grant GR/J60278, by ECHCM contract ERBCHRXCT940483, and by NATO Grant CRG1530959.

References

Brandenburg, A., Donner, K-J., 1997, to appear in Mon. Not. R. astr. Soc.
Brandenburg, A., Donner, K-J., Moss, D., Shukurov, A., Sokoloff, D.D., Tuominen, I., 1992, Astron. Astrophys. 259, 453
Buta, R., 1995, Astrophys. J. Suppl. Ser. 96, 39
Byrd, G., Rautiainen, P., Salo, H., Buta, R., Crocker, D.A., 1994, Astron. J. 108, 476
Chiba, M., 1991, Mon. Not. R. astr. Soc. 250, 769
Chiba, M., Lesch, H., 1994, Astron. Astrophys. 284, 731
Elstner, D., Meinel, R., Beck, R., 1992, Astron. Astrophys. Suppl. 94, 587
Friedli, D., Bentz, W., 1993, Astron. Astrophys. 268, 65
Lindblad, P.A.B., Kristen, H., 1996, Astron. Astrophys. 313, 733.
Lindblad, P.A.B., Lindblad, P.O., Athannasoula, E., 1996, Astron. Astrophys. 313, 65.
Little, B., Carlberg, R.G., 1991, Mon. Not. R. astr. 250, 161
Mestel, L., Subramanian, K., 1991, Mon. Not. R. astr. Soc. 248, 677
Moss, D., Brandenburg, A., 1992, Astron. Astrophys. 256, 371
Moss, D., Brandenburg, A., Donner, K-J., Thomasson, M., 1993a, Astrophys. J. 409,179
Moss, D., Brandenburg, A., Donner, K-J., Thomasson, M., 1993b, in "The Cosmic Dynamo", eds. F. Krause et al., Proc. IAU Symposium 157, 339
Moss, D., 1995, Mon. Not. R. astr. Soc. 275, 191
Moss, D., 1996a, Mon. Not. R. astr. Soc. 308, 381
Moss, D., 1996b, Mon. Not. R. astr. Soc. 315, 63
Moss, D., 1997, Mon. Not. R. astr. Soc. 289, 554
Moss, D., Tuominen, I., 1989, GAFD 49, 129
Otmianowska-Mazur, K., Chiba, M., 1995, Astron. Astrophys. 301, 41

Poezd, A.D., et al., 1993, Mon. Not. R. astr. Soc. 264, 285
Roberts, P.H., Soward, A.M., 1975, Astron. Nachr. 296, 49
Ruzmaikin, A.A., Shukurov, A.M., Sokoloff, D.D., 1988, Magnetic Fields of Galaxies (Dordrecht: Kluwer)
Ryder, S.D., Buta, R.J., Toledo, H., Shukla, H., Staveley-Smith, L., Walsh, W., 1996, Astrophys. J. 460, 665
Salo, H., 1991, Astron. Astrophys. 243, 118
Salo, H., Laurikainen, E., Astrophys. J. 410, 586
Schmidt, D., Rüdiger, G., Astron. Astrophys. 264, 319
Schwarz, M. P., 1981, Astrophys. J. 247, 77
Sellwood, J.A., 1981, Astron. Astrophys. 99, 362
Sellwood, J.A., Wilkinson, A.H., 1993, Rep. Prog. Phys. 56, 173
Sokoloff, D.D., Shukurov, A., 1990, Nature 347, 51
Subramanian, K., Mestel, L., 1993, Mon. Not. R. astr. Soc. 265, 649
Vainshtein, S.I., Zeldovich, Ya. B., 1972, Sov. Phys. Usp. 15, 159

This article was processed by the author using Springer-Verlag LaTeX A&A style file *L-AA* version 3.